Interferon-Induced Transmembrane Protein 3 Blocks Fusion of Diverse Enveloped Viruses by Altering Mechanical Properties of Cell Membranes

Xiangyang Guo, Jan Steinkühler, Mariana Marin, Xiang Li, Wuyuan Lu, Rumiana Dimova and Gregory B. Melikyan

Supplementary Figures, Figure Legends, Movie Legend and Appendix

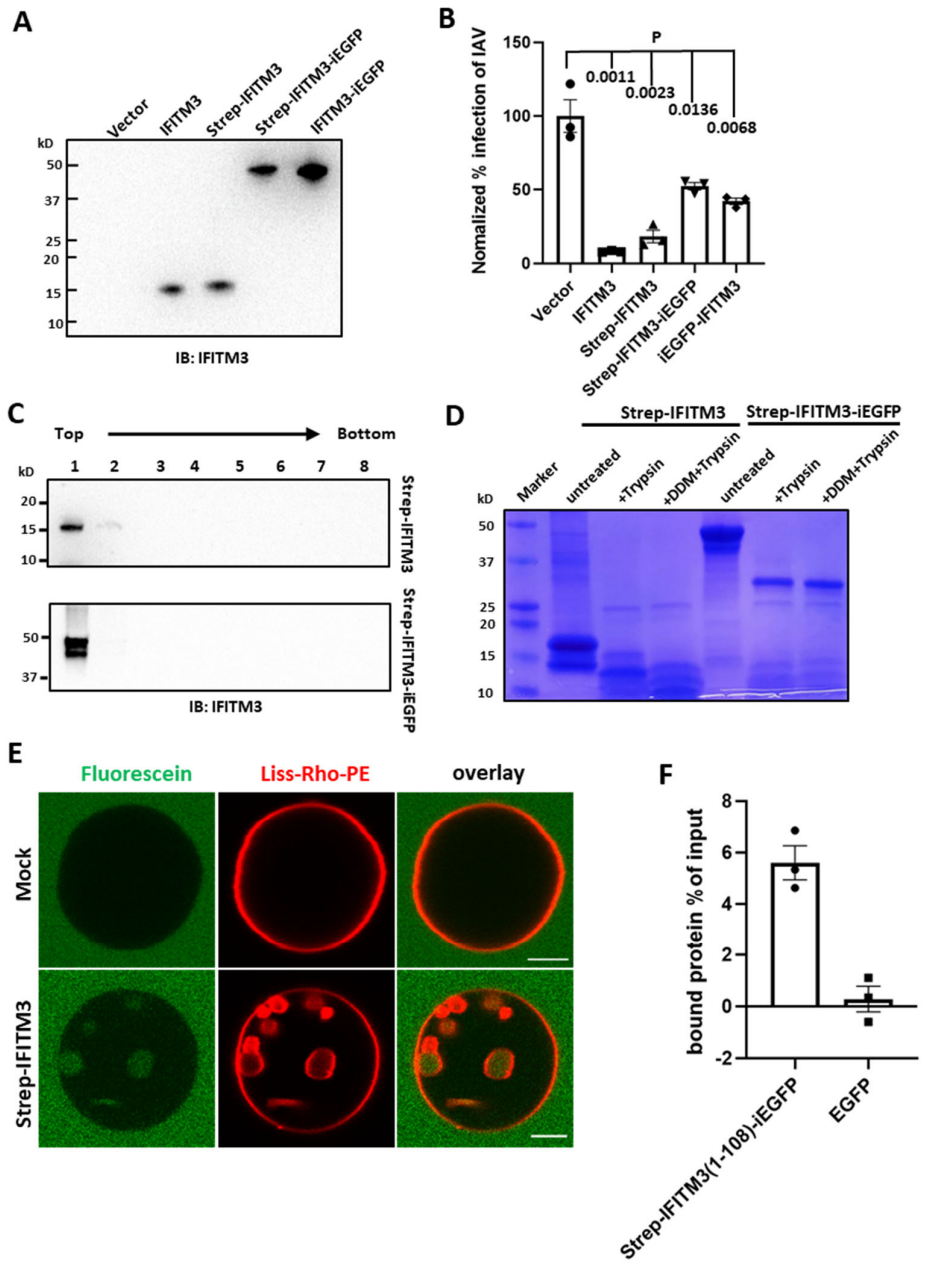

Figure S1. IFITM3 induces negative membrane curvature *in vitro*. (A) Expression levels of different IFITM3 constructs in transfected HEK 293T/17. HEK 293T/17 cells transfected with an empty Vector, unlabeled IFITM3, Strep-IFITM3, IFITM3-iEGFP, or Strep- IFITM3-iEGFP were lysed and analyzed by Western blotting using a rabbit antibody against the N-terminal region of IFITM3. (B) IAV pseudovirus infection is inhibited in HEK 293T/17 cells expressing IFITM3 constructs described in (A). The extent of infection by IAV pseudovirus carrying the luciferase gene measured by

luciferase activity is shown as a percentage of infection in cells transfected with empty vector. Data represent mean ± SEM (n = 3). (C) Strep-IFITM3 and Strep-IFITM3-iEGFP-reconstituted LUVs were subjected to floatation analysis. After density gradient centrifugation, collected fractions were analyzed by SDS–PAGE and Western blotting using rabbit anti-IFITM3 antibody. (D) Strep-IFITM3- and Strep-IFITM3-iEGFP-reconstituted LUVs were incubated with trypsin at 37 °C for 30 min. As a control, 0.2% n-Dodecyl-B-D-maltoside (DDM) was added with trypsin to permeabilize LUV membrane. The samples were analyzed by SDS-PAGE and stained with Coomassie blue. (E) Fluorescein (0.3 μM) was added to the external buffer of GUVs prepared from mock-treated LUVs (top) and from Strep-IFITM3-reconstituted LUVs (bottom) immediately after electroformation to mark *bona fide* inward budding events in GUVs. Scale bars 10 μm. (F) Membrane binding of Strep-IFITM3(1-108)-iEGFP assessed by a liposome co-sedimentation assay. Two mM of LUVs (99.0 mol % POPC, 0.5 mol % cholesterol, 0.5 mol % Liss-Rho-PE) were incubated at room temperature with 1 μM Strep-IFITM3(1-108)-iEGFP or EGFP for 10 min and then spun down by ultra-centrifugation. The bound % of protein was deduced from the reduction of EGFP fluorescence in supernatant and normalized by comparing with the fluorescence of input samples. Data represent mean ± SEM of the results of three independent experiments.

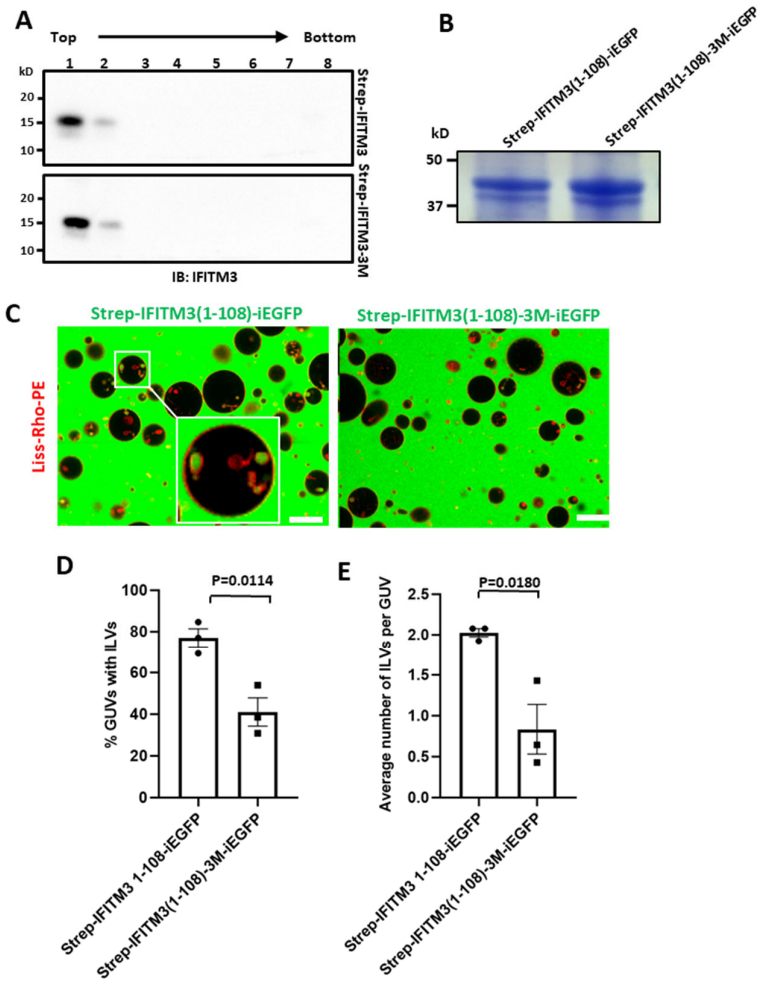

Figure S2. IFITM3 amphipathic helix is responsible for induction of negative membrane curvature. (A) Strep-IFITM3- and Strep-IFITM3-3M-reconstituted LUVs were subjected to floatation analysis. After density gradient centrifugation, collected fractions were analyzed by SDS–PAGE and Western blotting using rabbit anti-IFITM3 antibody. (B) Coomassie blue staining of purified Strep-IFITM3(1-108)-iEGFP and Strep-IFITM3(1-108)-3M-iEGFP. (C) GUVs (red) were incubated with 20 μM Strep-IFITM3(1-108)-iEGFP or Strep-IFITM3(1-108)-3M-iEGFP (green) for 30 min and imaged. Scale bars 10 μm. (D) Quantification of inward budding showing the percentage of GUVs, prepared and treated as in (C), with at least one intraluminal vesicle (ILV) containing EGFP. Data represent mean ± SEM of the results of three independent experiments, with 13 GUVs analyzed per sample in each experiment. (E) As in (D), but the plots represent the average number of ILVs per GUV.

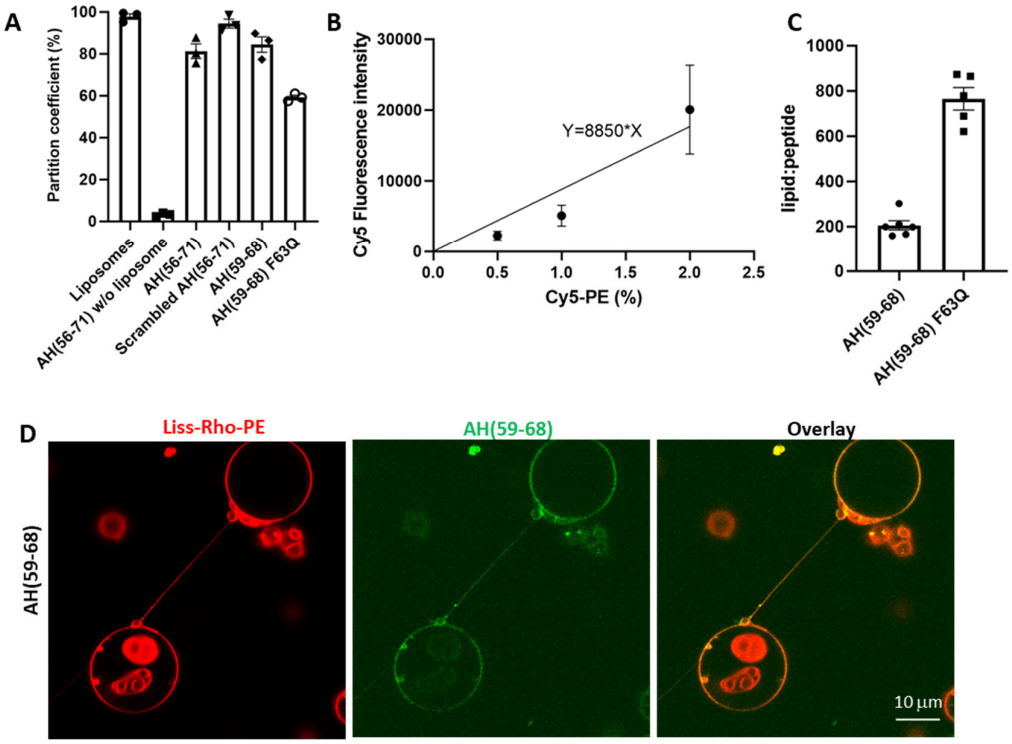

Figure S3. Membrane binding activity analysis of IFITM3 AH. (A) Partition coefficients of peptides. Two mM of LUVs (99.0 mol % POPC, 0.5 mol % cholesterol, 0.5 mol % Liss-Rho-PE) were incubated at room temperature with 40 µM of Cy5-labeled peptides for 10 min and spun down by ultra-centrifugation. The partition coefficient of peptides was deduced from reduction of Cy5 fluorescence in supernatant and normalized to the fluorescence input and is represented as % bound peptide relative to the input. Data represent mean ± SEM of the results of two independent experiments. Liposomes represents no-peptide control. (B) A standard curve of fluorescence intensity for varied concentrations of Cy5-PE incorporated in GUV membranes. Fluorescence intensity was analyzed by ImageJ using the Radial Profile Angle plugin. (C) Surface density of IFITM3 AH(59-68) and AH(59-68)F63Q on the GUV membrane was calculated by comparing the fluorescence intensity of the Cy5-conjugated AH with the standard curve in (B). (D) GUV tube-pulling assay was used to generate positively curved nanotubes. The AH(59-68) peptide (10 µM) was added after tube formation.

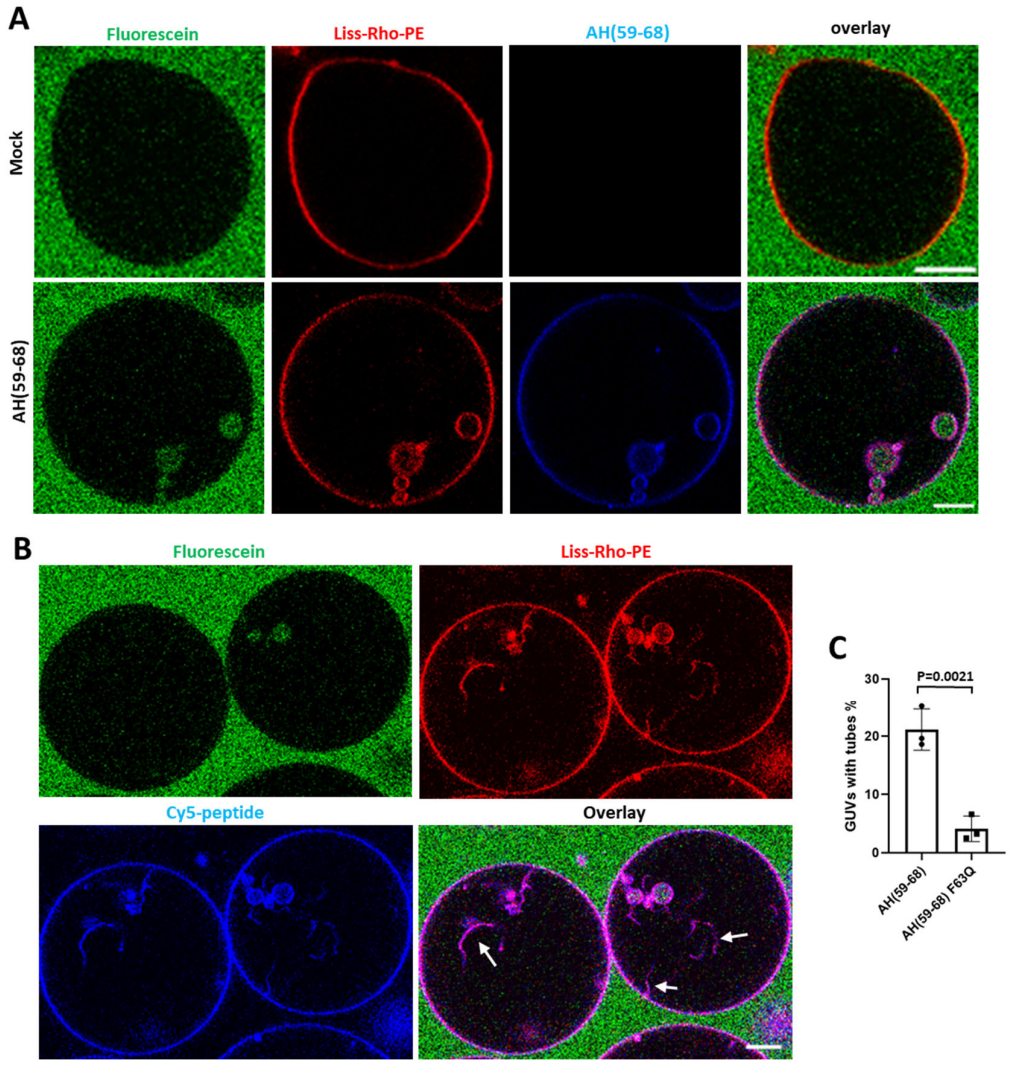

Figure S4. IFITM3 AH is sufficient to induce the formation of ILVs and nanotubes in GUVs. (A) GUVs prepared from a liver polar extract were treated with 10 μM AH(59-68) (bottom) or the same volume of DMSO (mock, top) for 30 min and imaged. Fluorescein (0.3 μM) was added to the external buffer to mark inward budding of GUVs occurring after electroformation. Scale bars 5 μm. (B) GUVs were treated with 10 μM AH(59-68) for 30 min and imaged. Fluorescein (0.3 μM) was added to the external buffer to mark inward budding of GUVs occurring after electroformation. Arrows indicate nanotubes. Scale bars 10 μm. (C) Percentage of GUVs, treated with 10 μM AH(59-68) or 10 μM AH(59-68)F63Q, with at least one nanotube that has AH-conjugated Cy5 fluorescence. Data represent mean ± SEM of the results of three independent experiments.

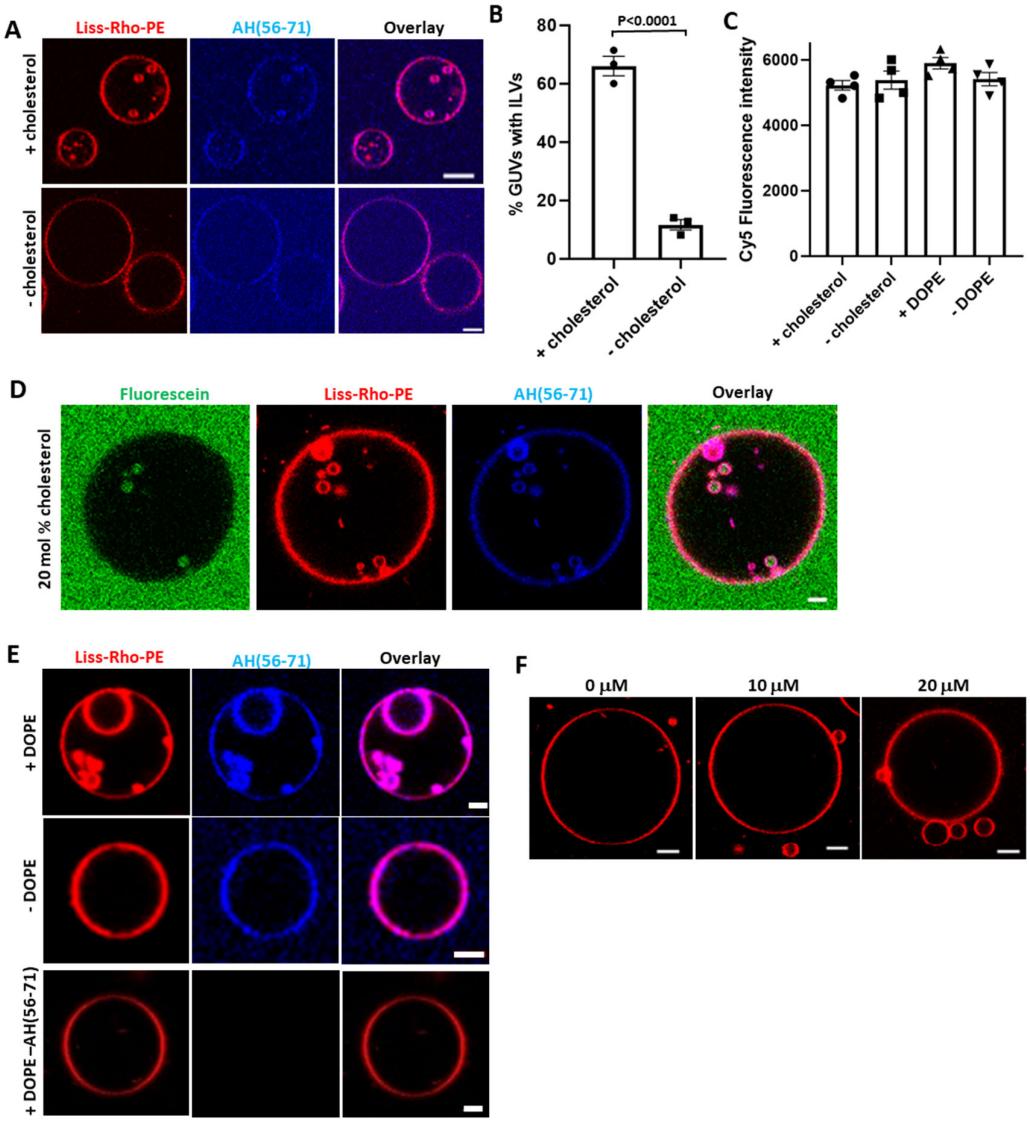

Figure S5. Negative membrane curvature induced by IFITM3 is facilitated by cholesterol, POPE and counteracted by lyso-lipids. (A) GUVs with cholesterol (99.0 mol % POPC, 0.5 mol % cholesterol, 0.5 mol % Liss-Rho-PE) or GUVs without cholesterol (99.5 mol % POPC, 0.5 mol % Liss-Rho-PE) were incubated with 10 µM AH(56-71) for 30 min and imaged. Scale bars 10 µm. (B) Quantification of inward budding showing the percentage of GUVs, prepared and treated as in (A), with at least one intraluminal vesicle (ILV) containing Cy5-labeled peptide. Data represent mean ± SEM of three independent experiments, with 45 GUVs analyzed per sample in each experiment. (C) Fluorescence intensity of Cy5-labeled AH(59-68) on the surface of GUVs ± cholesterol or GUVs ± DOPE, measured using the ImageJ Radial Profile

Angle plugin. (D) GUVs (79.5 mol % POPC, 20 mol % cholesterol, 0.5 mol % Liss-Rho-PE) were incubated with 10 μM AH(56-71) for 30 min and imaged. Scale bars 5 μm. (E) GUVs without POPE (99.0 mol % POPC, 0.5 mol % cholesterol, 0.5 mol % Liss-Rho-PE) or with POPE (79.5 mol % POPC, 20 mol % DOPE, 0.5 mol % Liss-Rho-PE) were incubated with 10 μM AH(56-71) for 30 min and imaged. Scale bars 5 μm. (F) GUVs (99.0 mol % POPC, 0.5 mol % cholesterol, 0.5 mol % Liss-Rho-PE) were treated with an indicated concentration of LPC for 30 min and imaged. Scale bars 10 μm.

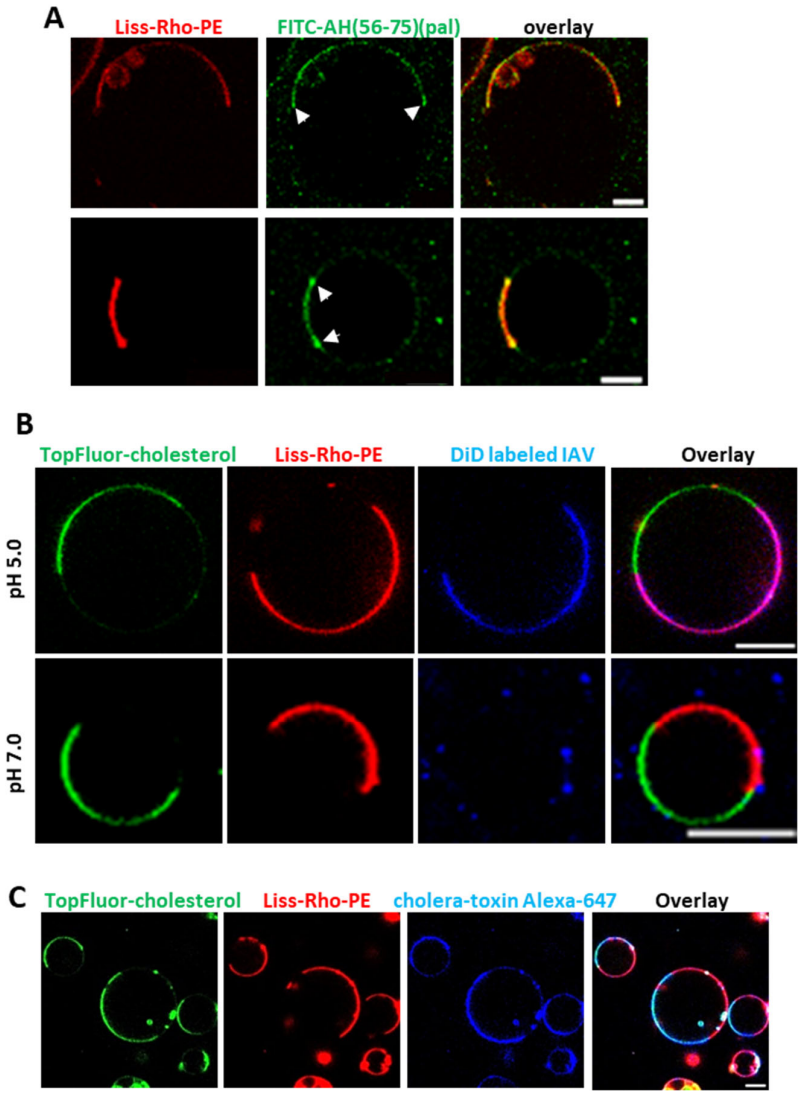

Figure S6. IFITM3 partitions into liquid-disordered membrane domains that support IAV fusion. (A) Shown are two examples of phase-separated GUVs (33.3 mol % DOPC, 33.3 mol % SM, 32.4 mol % cholesterol, 0.5 mol % TopFluor-cholesterol and 0.5% Liss-Rho-PE) incubated with 10 μM of FITC-labeled palmitoylated AH (FITC-AH(56-75)(pal)) for 30 min. Arrows indicate accumulation of FITC-AH(56-75)(pal) peptide at the phase boundary. Scale bars 5 μm. (B) Phase-separated GUVs (33.3 mol % DOPC, 33.3 mol % SM, 30.4 mol % cholesterol, 2% GM1, 0.5 mol % TopFluor-cholesterol and 0.5% Liss-Rho-PE) were mixed with DiD-labeled IAV. Lipids mixing between IAV and GUV was triggered by addition of a predetermined amount of citrate buffer to achieve the final pH of 5.0 and samples were immediately imaged. PBS (pH 7.2) was used as control. Scale bars 10 μm. (C) GM1 in phase-

separated GUVs (33.3 mol % DOPC, 33.3 mol % SM, 30.4 mol % cholesterol, 2% GM1, 0.5 mol % TopFluor-cholesterol and 0.5% Liss-Rho-PE) was stained with cholera-toxin B Alexa-647. Scale bars 10 μm.

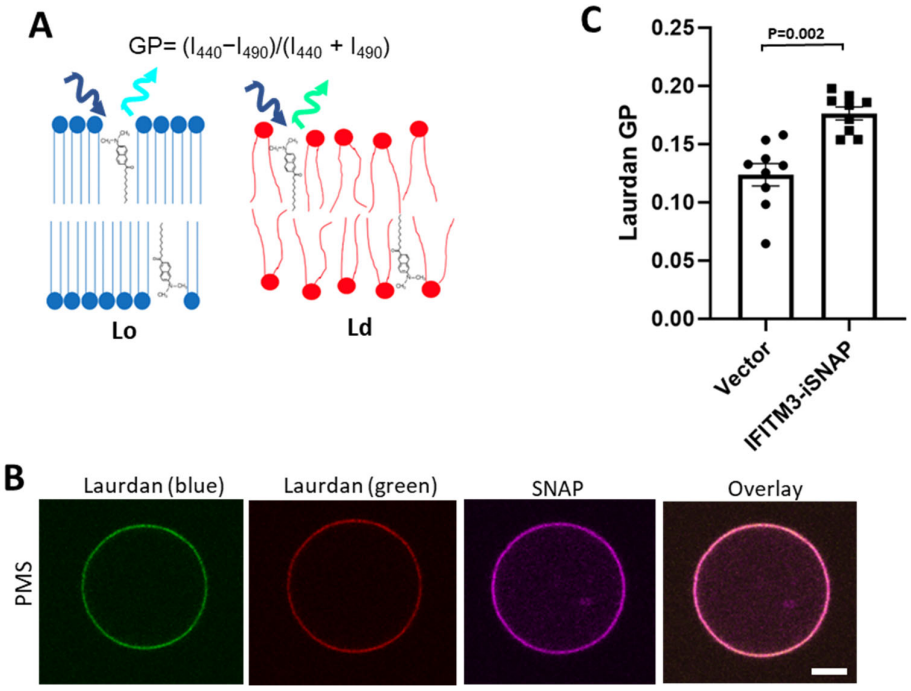

Figure S7. Full-length IFITM3 increases lipid order. (A) A diagram illustrating the principle of Laurdan-based measurements of lipid order. (B) Plasma membrane spheres were prepared from IFITM3-iSNAP expressing A549 cells by cell swelling and stained with SNAP-cell 647-SIR (violet) for SNAP and treated with Laurdan for lipid order measurement. The Laurdan fluorescence signal was acquired from 419 nm to 464 nm for the blue channel and from 472 nm to 517 nm for the green channel. Scale bars 10 μm. (C) General Polarization (GP) of Laurdan was calculated using the equation $GP= (I_b−I_g)/(I_b + I_g)$ (I_b and I_g represent Laurdan fluorescence from the blue channel and the green channel, respectively) based on the ratio of Laurdan fluorescence of plasma membrane spheres prepared from IFITM3-iSNAP expressing A549 cells and cells transduced with empty vector (control). Data represent mean ± SEM of at least three independent experiments.

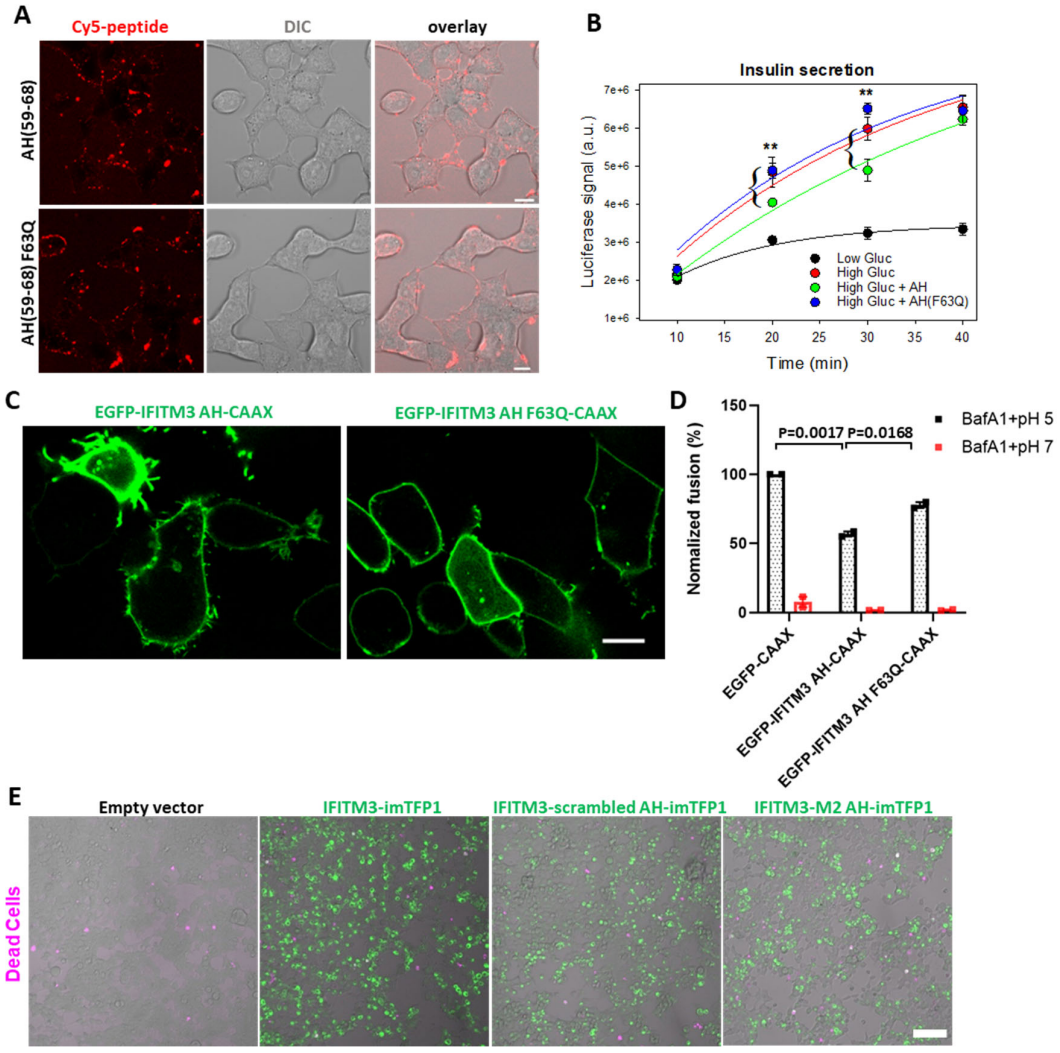

Figure S8. IFITM3 AH is sufficient to inhibit membrane fusion. (A) INS-1E cells were treated with 5 μM AH(59-68) or 10 μM AH(59-68)F63Q for 5 min and imaged. Scale bars 10 μm. (B) Time course of glucose-stimulated insulin secretion in INS-1E cells transduced with proinsulin-luciferase fusion construct. INS-1E cells were preincubated for 5 min with 5 μM AH(59-68) or 10 μM AH(59-68)F63Q and stimulated for 20 min with a high glucose (20 mM, HG) or low glucose (2.8 mM, LG) buffer as control. Luciferase activity was measured for each time point by adding the coelenterazine substrate to the supernatant and reading on a Luminescence counter. Data represent mean ± SD of the results of two independent experiments. **, $p<0.01$ for HG and HG + AH(59-68) samples. (C) 293T cells expressing EGFP-IFITM3 AH-CAAX or EGFP-IFITM3 AH F63Q-CAAX (green). Scale bar 10 μm. (D) Forced

fusion of IAV/BlaM-Vpr pseudoviruses at the plasma membrane of A549 cells expressing either EGFP-CAAX, or EGFP-IFITM3 AH-CAAX or EGFP-IFITM3 AH F63Q-CAAX. Fusion of cell-bound viruses was induced by exposure to a pH 5.0 buffer, as described in Methods. Data represent mean ± SEM of two independent experiments, each in triplicates. (E) HEK 293T/17 cells expressing wild-type or scrambled imTFP1-tagged IFITM3 or IFITM3 M2 AH chimera were infected by IAV and cell viability was tested using a LIVE/DEAD™ Fixable Far Red Dead Cell Stain Kit 12 h after infection. Dead cells are shown in magenta. Scale bar 100 μm.

Supplemental Table 1. Key resources.

REAGENT or RESOURCE	SOURCE	IDENTIFIER
Antibodies		
Rabbit anti IFITM3 (N-term) antibody	Abgent	AP1153a
Bacterial and Virus Strains		
Rosetta™ 2 (DE3) pLysS Singles™	MilliporeSigma	Cat#71401-M
NEB® 5-alpha Competent E. coli	New England Biolabs	Cat#C2987H
Influenza A/PR/8/34(HIN1)	Charles River Laboratories	Cat#10100374
PR8-mCherry H1N1 IAV	PMID: 28798254	N/A
Chemicals, Peptides, and Recombinant Proteins		
Streptavidin, Alexa Fluor™ 647 conjugate	Thermo Fisher Scientific	Cat#S21374
Streptavidin	Thermo Fisher Scientific	Cat#PI21125
BSA-Biotin	Thermo Fisher science	Cat#29130
Cholera Toxin Subunit B (Recombinant), Alexa Fluor 647	Thermo Fisher Scientific	Cat#C34778
ANAPOE-X-100	Anatrace	Cat#APX100
BioBeads SM-2 absorbent beads	Bio-Rad	Cat#1528920
POPC	Avanti Polar Lipids	Cat#850457
DOPC	Avanti Polar Lipids	Cat#850375
DOPE	Avanti Polar Lipids	Cat#850725
18:1 Biotinyl Cap PE	Avanti Polar Lipids	Cat#870273
18:0 Lyso PC	Avanti Polar Lipids	Cat#855775
18:0 SM	Avanti Polar Lipids	Cat#860586
cholesterol (ovine)	Avanti Polar Lipids	Cat#700000
Ganglioside GM1 (Ovine Brain)	Avanti Polar Lipids	Cat#860065
TopFluor® Cholesterol	Avanti Polar Lipids	Cat#810255
Liver Extract Polar	Avanti Polar Lipids	Cat#181108
DiD solid	Thermo Fisher Scientific	Cat#D7757
cOmplete EDTA-free Protease Inhibitor Cocktail	Roche	Cat#11873580001
Bafilomycin A1	Sigma	Cat#B1793-10UG
Rabbit anti IFITM3 (N-term) antibody	Abgent	AP1153a
Strep-Tactin Superflow Plus	Qiagen	Cat#30004
CCF4-AM	Invitrogen	Cat#K1095
Experimental Models: Cell Lines		
HEK293T/17	ATCC	ACS-4500
A549	ATCC	CCL-185
INS-1E	Addexbio Technologies	Cat#C0018009
Recombinant DNA		
pQCXIP	Takara Bio USA, Inc.	Cat#631515
Proinsulin-NanoLuc	Addgene PMID: 25565210	Cat#62057
psPAX2	Addgene	Cat#12260
pMD2.G	Addgene	Cat#12259
pCAGGS HA WSN/33	PMID: 22046135	N/A
pCAGGS NA WSN/33	PMID: 22046135	N/A
pNL4-3.Luc.R–E–	NIH AIDS Reagent Program	Cat#3418
pcRev	NIH AIDS Reagent Program	Cat#11415

pR9ΔEnv	PMID: 29649444	
Software and Algorithms		
Fiji/ImageJ	https://imagej.nih.gov/ij/docs/guide/146-2.html	RRID:SCR_002285
Graphpad	https:www.graphpad.com/	N/A

Supplemental Video S1. 3D image series of GUVs containing ILVs and nanotubes. Movie shows z-stacks of a Strep-IFITM3-iEGFP (green)-reconstituted GUV (labeled with Liss-Rho-PE, red) scanned from bottom to top with a z-section interval of 0.2 µm. Scale bar 10 µm.

Supplemental Appendix

AH(59-68) was observed to induce nanotubes (cylindrical or neckless-like structures of high curvature below the optical resolution) in the GUV lumen (Figs. 2B and S4B, movie S1). This observation was used to obtain an order-of-magnitude estimate of the membrane curvature generated by the AH(59-68) peptide. This estimate was then compared to other membrane curvature inducing proteins.

The widely used curvature elasticity model implies a membrane spontaneous curvature of $m = -c * 1/R_{tube}$ with a pre-factor c of 1/2 or 1 for homogenous lipid bilayers that form GUVs with coexisting inward-pointing nanotubes.[1] As in our experiments the exact radius R_{tube} of the tubes cannot be resolved, we take the optical resolution limit (250 nm) as an upper limit for the tube diameter $2*R_{tube}$. By taking c=1/2, we obtain a lower limit for the spontaneous curvature generated by AH(59-68).[2] In the dilute regime, where peptide-peptide interactions are neglectable, one can consider the curvature generated per peptide as $m = \phi * m_0$, where ϕ is the membrane area fraction occupied by the peptide. To estimate ϕ from fluorescence measurements showing that 1 peptide is bound per 100 lipid molecules of the external leaflet of GUV (Fig. S3B, C), we approximated the footprint of the alpha-helical peptide on the membrane as a flat cylinder at the lipid-water interface (1.8 nm^2) and assumed 0.7 nm^2 for area per lipid molecule.

We find $m_0^{-1} \approx -6.4$ nm, which is comparable to the membrane curvature generated by amphiphysin 1 in the dilute regime.[3] However, while AH(59-68) induces negative curvature, amphiphysin 1 generates positive curvature. Thus, the effect of AH(59-68) might be better compared to I-BAR protein, which was also found to have a similar value of m_0 of same sign.[4] Compared to the literature values, our estimate is based only on a single protein density and has larger uncertainties. However, as the calculations varies only linearly in respect to the experimental uncertainties, we remain confident about the order of magnitude for our estimate of m_0.

We note that the estimate for m_0^{-1} is comparable to the bilayer thickness, which is the relevant length-scale for bilayer stalk formation and fusion. In summary, we conclude that the local ("intrinsic") curvature generated by AH(59-68) is rather large, comparable to that for established physiological curvature-inducing proteins. This curvature should have a major contribution to the energetics of membrane remodeling, even at dilute concentrations and on smaller scales than is directly observable in the GUV experiments.

REFERENCES

(1) Li, Y. H.; Lipowsky, R.; Dimova, R., Membrane Nanotubes Induced by Aqueous Phase Separation and Stabilized by Spontaneous Curvature. *P Natl Acad Sci USA* **2011,** *108*, 4731-4736.

(2) Steinkuhler, J.; Knorr, R. L.; Zhao, Z. L.; Bhatia, T.; Bartelt, S. M.; Wegner, S.; Dimova, R.; Lipowsky, R., Controlled Division of Cell-Sized Vesicles by Low Densities of Membrane-Bound Proteins. *Nature Communications* **2020,** *11*.

(3) Sorre, B.; Callan-Jones, A.; Manzi, J.; Goud, B.; Prost, J.; Bassereau, P.; Roux, A., Nature of Curvature Coupling of Amphiphysin with Membranes Depends on Its Bound Density. *P Natl Acad Sci USA* **2012,** *109*, 173-178.

(4) Chen, Z.; Shi, Z.; Baumgart, T., Regulation of Membrane-Shape Transitions Induced by I-BAR Domains. *Biophys J* **2015,** *109*, 298-307.